

Regular paper

**Performance of Controlled FACTS and
VSC-HVDC in a Power System Subject to Inter-Area Oscillation**

Ahmed S. Al-ahmed

King Fahd University of Petroleum and Minerals,
Saudi Arabia



*Journal of Automation
& Systems Engineering*

Abstract- The rapid expansion of power systems and diversity of power generation sources have surfaced the necessity of improving the current conventional grid to a smarter, more flexible and more controllable one. These improvements are ultimately achieved by the implementation of the concepts of Flexible Alternating Current Transmission Systems (FACTS) devices and High Voltage Direct Current (HVDC) technologies. Most power systems nowadays are considering these technologies however their performance might not comply with the expected utmost performance. This paper shows the improvement of transient stability and Power Oscillation Damping (POD) when FACTS and HVDC are implemented and controlled. Three control signals will be studied and designed on each device. Two control strategies will be used the first is based on residue method and the second is based on Control Layapunov Function (CLF). Simulation results of the system with and without controllable components will be presented and examined. A comparison between the control signals will also be displayed.

Keywords: Control Layapunov Function (CLF), Flexible AC Transmission Systems (FACTS), High Voltage DC (HVDC), Lead-lag Filters, Modal Analysis, Power Oscillation Damping; Residue Method, Single-Machine-Equivalent-method (SIME), TCSC, SVC

Article history: Received 21 December 2017, Accepted 8 February 2018.

1. INTRODUCTION

FOR MANY years, the typical power system has served as the backbone of the process of transmitting power from generators to consumers. However, the growing number of distributed (decentralized) power plants and the orientations to interconnect local and cross-border power systems have led to more fluctuations in the system. These fluctuations are usually caused by the electromechanical oscillations of synchronous generator rotors against each other [7]. Moreover, the system became more congested and thus more vulnerable to power outages and less robust towards faults and instabilities. As a result, the need of having a more dynamic system that has a greater controllability in which the power-flow can be monitored effectively and a proper damping of oscillations can be achieved is essential. This upgrade in the system can be done by using fast-response controllers. Flexible AC Transmission system (FACTS) provides a resilient system where currents and voltages can be swiftly controlled to ensure a proper power-flow. Furthermore, in Voltage-source converter (VSC) based HVDC the system is usually less expensive since it requires less conductors per area [14]. Also, VSC-HVDC provides a robust and independent control over active and reactive power ensuring an increased transmission flexibility and capability [4]. In this work, we aim to scrutinize the impact of FACTS devices and VSC-HVDC systems in achieving the required stability and damping of

electromechanical oscillations. The devices and systems will be controlled using a signal known as Power Oscillation Damping (POD) signal which will be designed based on residue method and Control Layapunov Function (CLF). The first control strategy to improve the damping of power oscillations is to perform modal analysis and linearize the system using the digital simulator tool: Simulation of POWER systems (SIMPOW) [9]. The parameters of the POD are then tuned by employing the residue method discussed in [11]. The second control strategy which is based on CLF is frequently used to control nonlinear systems [8]. Many research papers in the field do not combine the two concepts of FACTS and VSC-HVDC and subject them to different control strategies and signals to compare between them in their level of efficiency and hence improving the transient stability and damping of the system.

This paper is organized as follows. Section II is devoted to the modeling of the controllable devices that will be used in the simulation, while Section III presents an elaboration of the different control techniques used along with a brief theoretical framework about them. Section IV shows the simulation results and a thorough comparison between the used methods. Section V and VI involve the conclusion and references, respectively.

2. MODELLING OF CONTROLLABLE DEVICES

Two FACTS devices (TCSC, SVC) and an HVDC (VSC) system will be used to enhance the damping of the network. A mathematical modeling for each device is provided in this section.

2.1 Thyristor Controlled Series Compensator (TCSC)

This controllable reactance is sometimes referred to as thyristor controlled series capacitor and from its name it is connected in series with the transmission line [4]. Installation of TCSC grants a higher transfer of power with control over the direction of power-flow [10]. As shown in Fig.1, A TCSC consists of a conventional fixed capacitor connected in parallel with a thyristor controlled reactance. The total reactance of the configuration is controlled by changing the firing angle of the thyristor.

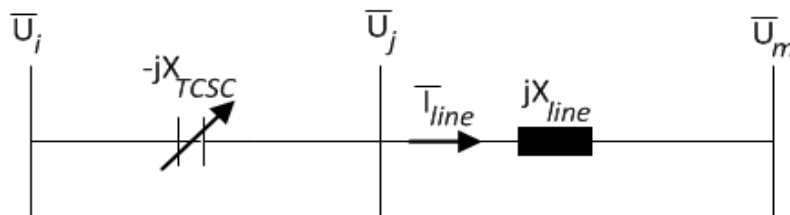


Figure 1 Steady-state model of TCSC.

The power-flow through the lossless transmission line between the two busses depicted in Fig.1 is as follows:

$$P_{ij} = \frac{U_i U_j}{X_{tot}} \sin(\theta_{ij})$$

$$Q_{ij} = (U_i^2 - U_i U_j \cos(\theta_{ij})) / X_{tot} \quad (1)$$

where,

$$X_{tot} = X_{line} - X_{TCSC} \quad (2)$$

$$\theta_{ij} = \theta_i - \theta_j \quad (3)$$

The inverse relationship in (1) indicates that the less the total reactance (X_{tot}) is, the more the active power (P_{ij}) is transmitted between the two busses. This tight relevance between line reactances and the active power reveals the capabilities of TCSCs to damp

electromechanical oscillations. To enhance the damping and make it more robust, a proper input signal and control laws need to be applied [8]. The reactance (X_{TCSC}) can be automatically adjusted between a minimum and maximum value by the PI controller to obtain a specific control mode.

$$X_{TCSC}^{min} \leq X_{TCSC} \leq X_{TCSC}^{max} \quad (4)$$

The dynamic model of TCSC for transient stability and small signal study is depicted in Fig. 2.

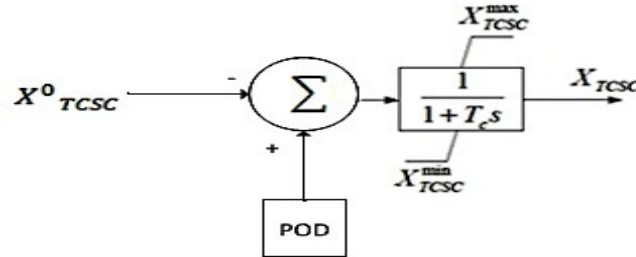


Figure 2 Dynamic model of TCSC.

2.2 Static Var Compensator (SVC)

The voltage in transmission line areas that are relatively far from generator busses suffers from the line impedance effect which is usually inductive. This will lead to a phenomenon known as under-voltage. To overcome this reduction in voltage, a Static Var Compensator (SVC) is placed to compensate for reactive loads in the busses that are at a great distance from the generator busses. As a result, SVCs have the capability to control the voltage since they can generate and absorb reactive power. SVCs have no rotating components, it only consists of a fixed capacitor bank that is regulated to supply the maximum required capacitive reactive power [3]. A controlled thyristor is also attached so that the excessive instantaneous reactive power is properly consumed. As shown in Fig.3, the SVC is in principle a controlled shunt susceptance and can be represented by the following equation :

$$U = U_{ref} \mp \frac{I_{SVC}}{B_{SVC}} \quad (5)$$

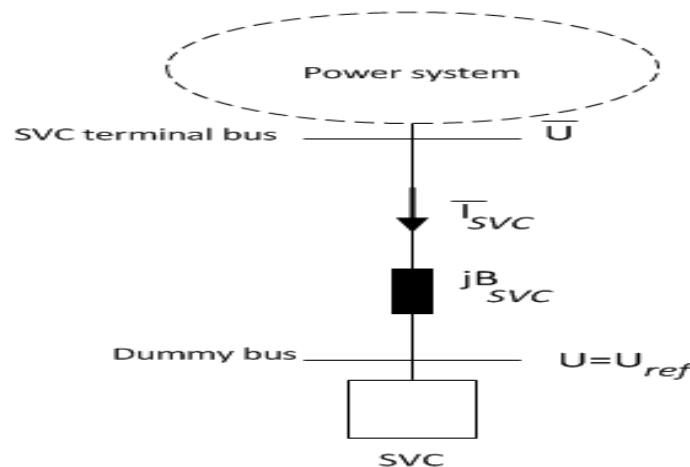


Figure 3 Simple model of SVC.

Where the negative sign and positive sign represent capacitive and inductive currents, respectively. U_{ref} is the reference voltage magnitude of the SVC bus at $I_{SVC} = 0$. The

amount of reactive power of the SVC is:

$$Q_{SVC} = -B_{SVC}U^2 \quad (6)$$

The shunt admittance (B_{SVC}) can be varied between a minimum and maximum value, absorbing or generating reactive power to regulate the voltage.

$$B_{SVC}^{min} \leq B_{SVC} \leq B_{SVC}^{max} \quad (7)$$

Fig.4 shows the dynamic model of SVC for transient stability and small signal.

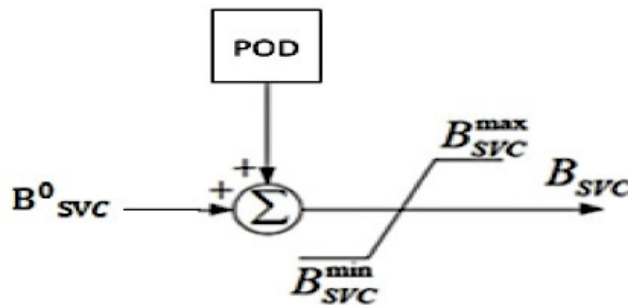


Figure 4 Dynamic model of SVC

2.3 Voltage Source Converter Based High Voltage Direct Current (VSC-HVDC)

HVDC's main feature is the ability to independently control the active and reactive power in case of interconnection between AC networks [5]. Furthermore, HVDC allows more power to be transferred. VSCs in principle are based on valves that connect and disconnect according to a control signal. New voltage magnitudes and angles can be achieved by using pulse width modulation(PWM) which is possible to use when high switching frequency components are present. A simple VSC-HVDC transmission model in parallel with an AC transmission line is presented in fig.5.

$$\bar{E}_{Ci} = E_{Ci}e^{j\gamma_i} \quad \bar{E}_{Cj} = E_{Cj}e^{j\gamma_j} \quad (8)$$

Where E_{Ci} , E_{Cj} , γ_i , γ_j are the controllable variables, magnitude and phase angles of the voltage sources, respectively.

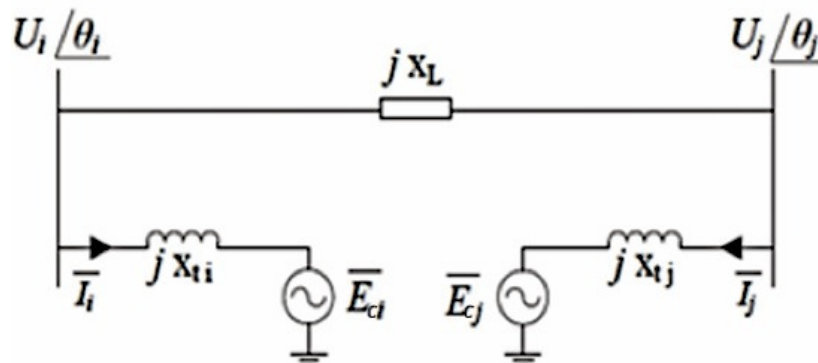


Figure 5 Simple VSC-HVDC transmission model.

x_{ti} and x_{tj} denotes the reactances of the power transformers. These variables of the SVC can be controlled with respect to the AC supply voltage waveform to supply both active and reactive power to the AC system. By assuming that the losses of the converters are constant, the losses then can be represented as a constant load. One can redraw Fig.5,

neglecting the losses of the DC cables as shown in Fig.6.

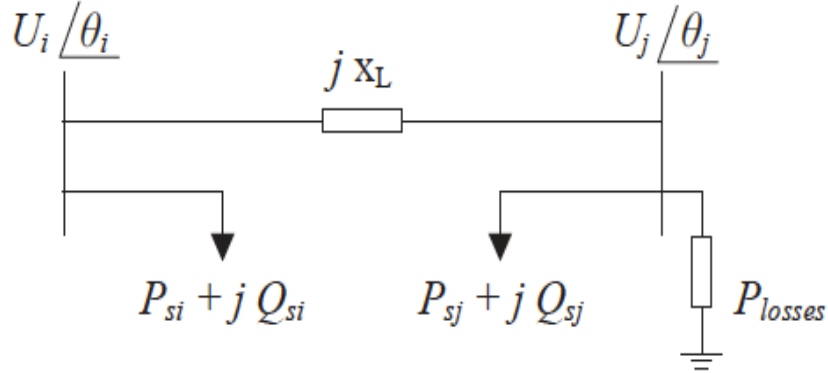


Figure 6 Injection model of VSC-HVDC transmission.

The injected active and reactive power into the VSCs is as follows:

$$\begin{aligned} P_{si} &= b_{ti} U_i (\sin \theta_i u_{pi} - \cos \theta_i u_{qi}) \\ Q_{si} &= b_{ti} [U_i^2 - U_i (\cos \theta_i u_{pi} + \sin \theta_i u_{qi})] \end{aligned} \quad (9)$$

$$\begin{aligned} P_{sj} &= b_{tj} U_j (\sin \theta_j u_{pj} - \cos \theta_j u_{qj}) \\ Q_{sj} &= b_{tj} [U_j^2 - U_j (\cos \theta_j u_{pj} + \sin \theta_j u_{qj})] \\ P_{si} &= -P_{sj} \end{aligned} \quad (10)$$

Where,

$$\begin{aligned} u_{pi} &= E_{Ci} \cos \gamma_i & u_{qi} &= E_{Ci} \sin \gamma_i \\ u_{pj} &= E_{Cj} \cos \gamma_j & u_{qj} &= E_{Cj} \sin \gamma_j \end{aligned} \quad (11)$$

From equations 10 & 11, it can be deduced that P_{si} and Q_{si} can be controlled by E_{Ci} and γ_i . Similarly, P_{sj} and Q_{sj} can be controlled by E_{Cj} and γ_j . Due to the controllability of the voltage magnitude and angle, it is possible to implement two integrator controllers in each converter, one for active power and one for reactive power.

3. CONTROL STRATEGIES

To monitor the preceding devices and hence improve the Power Oscillations Damping (POD) some control strategies need to be applied.

3.1 Modal Analysis

Modal analysis method depends on linearizing the dynamic of the power system which is symbolized by a set of nonlinear Differential-Algebraic Equations (DAE).

$$\begin{aligned} \dot{x} &= f(x, y, u) \\ 0 &= g(x, y, u) \end{aligned} \quad (12)$$

where x, y and u are vectors containing the state, algebraic and input variables of the system, respectively. By linearizing the aforementioned equation around its equilibrium point, the stability of the system can be performed using its eigenvalues [6]. The linearized system is characterized by four matrices symbolizing the Linear Time-Invariant (LTI) system below.

$$\Delta \dot{x}(t) = A \Delta x(t) + B \Delta u(t)$$

$$\Delta y(t) = C \Delta x(t) + D \Delta u(t) \quad (13)$$

where A is the state matrix, B and C are the input and output matrices, respectively. D is the feed-forward matrix. The terms $\Delta x(t)$, $\Delta y(t)$ and $\Delta u(t)$ represent the change in state, output and input variables, respectively.

The eigenvalues (λ) of the system are found using the state matrix A as the following:

$$\det (A - \lambda \mathbf{1}) = 0 \quad (14)$$

where *det* stands for the determinant of the matrix and $\mathbf{1}$ is the unity matrix. These eigenvalues are defined, in modal analysis, as the modes of the system.

$$\lambda_i = \sigma_i + j\omega_i \quad (14.A)$$

where *i* is the mode number. From the real and imaginary part of the eigenvalue, the frequency (f_{pi}) and damping ratio (ξ_i) of the system can be obtained as follows:

$$\begin{aligned} f_{pi} &= \frac{\omega_i}{2\pi} \\ \xi_i &= -\frac{\sigma_i}{|\lambda_i|} \end{aligned} \quad (15)$$

As illustrated in [6], the damping of the system has to be positive in order for it to be stable. However, the modes containing a small positive value of damping ratio can be reduced until reaching a negative value in the case of disturbances. These poorly damped modes which fall under the category of inter-area modes where the modes of interest, in our case, lie in the frequency range between 0.1 to 2 Hz. The level of how well a mode is observed is called the observability (O) of a mode. Thus, the higher the number of observability is, the clearer the mode is observed in the output. The derivation of the equation of observability is introduced in [8] and it is as follows:

$$O_{ij} = \frac{|c_j v_i^r|}{\|c_j\| \|v_i^r\|} \quad (16)$$

Where v_i^r is the right eigenvector associated to the *i*-th mode. Moreover, the level of how well a mode is controlled is called the controllability (Cl_i) of a mode and it is defined, from [8], as the following:

$$Cl_{ij} = \frac{|B_j (v_i^l)^T|}{\|B_j\| \|v_i^l\|} \quad (17)$$

Where v_i^l is the left eigenvector associated to the *i*-th mode.

3.2 Residue Method

Starting by deriving the transfer function of the LTI system in (13), the following partial function is acquired:

$$G(s) = \frac{\Delta y(s)}{\Delta u(s)} = \sum_{i=1}^{n_x} \left(\frac{\bar{R}_i}{s - \lambda_i} \right) \quad (18)$$

where \bar{R}_i is the residue of the system at the eigenvalue λ_i and is shown as:

$$\bar{R}_i = Cv_i^r v_i^l B \quad (19)$$

The open-loop system in (18) can be closed (Fig.7) by attaching a feedback transfer function (H) of the form $H(s,K) = K H(s)$, where K is the gain of the system [2]. Thus, in order to improve the damping of power oscillations by designing a POD for controllable devices, the following equation is used:

$$\frac{\Delta\lambda_i}{\Delta K} = \bar{R}_i H(\lambda_i) \quad (20)$$

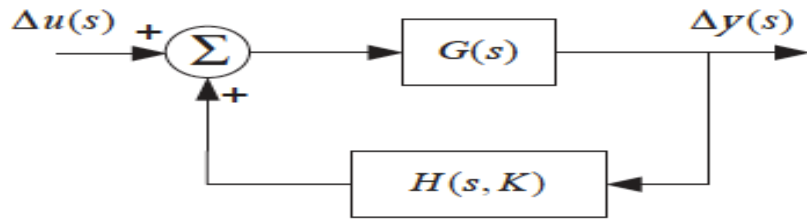


Figure 7 Closed-loop system.

The POD signal can be inserted at different positions in the regulator. The residue method is used to obtain the POD signal by tuning the lead-lag filters of the linearized system (Fig.8).

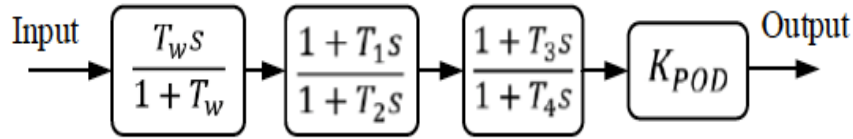


Figure 8 regulator of a linear pod.

According to Fig.8, the POD consists of a washout filter (T_w) that passes only the high signals where oscillations occur. The second and third blocks are called the lead-lag filters (n_f) and are used as phase compensators. The last block (K_{POD}) represents the gain that is modified to keep the signal within allowable limits. The approach in [11] will be used to find the lead-lag filter parameters. The aim of the POD is to shift the eigenvalues from right to left plane without changes on the imaginary axis (Fig.9). In other words, decreasing the real part of the eigenvalue and keeping the imaginary part constant, thus improving the damping. The angle (ϕ) is set as in (21) assuring that the result of residual and feedback transfer function are negative.

$$\phi = \pi - \arg(\bar{R}_i) \quad (21)$$

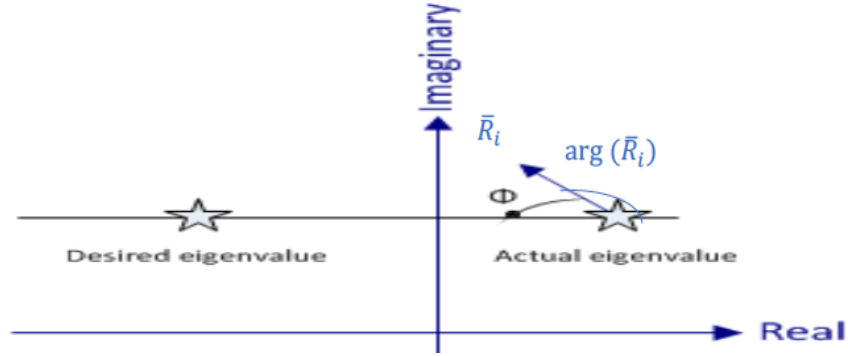


Figure 9 Eigenvalue departure direction for a minor change of system parameters.

The number of lead-lag filters depends on the angles (ϕ) as shown below:

$$\begin{aligned} 0 < |\phi| \leq 60 & \stackrel{\text{Then}}{\Rightarrow} n_f = 1 \\ 60 < |\phi| \leq 120 & \stackrel{\text{Then}}{\Rightarrow} n_f = 2 \\ 120 < |\phi| \leq 180 & \stackrel{\text{Then}}{\Rightarrow} n_f = 1 \\ \text{set } \phi & = -\arg(\bar{R}_i), \quad K_{POD} = K_{POD}e^{j\pi} \end{aligned} \quad (22)$$

The parameters ($T_1 - T_4$) of the lead-lag filter (n_f) are adjusted so that a positive contribution to damping is achieved:

$$\begin{aligned} T_1 & = \alpha T, \quad T_2 = T \\ T_3 & = T_4 = 1, \text{ when } n_f = 1 \\ T_3 & = T_1, \quad T_4 = T_2, \text{ when } n_f = 2 \end{aligned} \quad (23)$$

where,

$$\alpha = \frac{1 + \sin\left(\frac{\phi}{n_f}\right)}{1 - \sin\left(\frac{\phi}{n_f}\right)}, \quad T = \frac{1}{\omega_p \sqrt{\alpha}} \quad (24)$$

The output signal of the system which will be used to tune the POD can be a local signal or a global signal, e.g. active power in a line and the rotor angle speed (ω^{SIME}) in a Single Machine Equivalent model (SIME).

SIME method allows easier investigation of power systems by replacing multi-machine systems by a system that has two distinct machine groups: critical machines (C) and non-critical machines (NC). By definition, critical machines are the ones responsible for the loss of synchronism. The new single machine equivalent rotor angle (δ^{SIME}) and rotor speed (ω^{SIME}) are as follows:

$$\delta_{SIME} = \delta_C - \delta_{NC} = \frac{\sum_{i \in C} M_i \delta_i}{\sum_{i \in C} M_i} - \frac{\sum_{j \in NC} M_j \delta_j}{\sum_{j \in NC} M_j}$$

$$\omega_{SIME} = \omega_C - \omega_{NC} = \frac{\sum_{i \in C} M_i \omega_i}{\sum_{i \in C} M_i} - \frac{\sum_{j \in NC} M_j \omega_j}{\sum_{j \in NC} M_j} \quad (25)$$

Where, M_C and M_{NC} are the total inertia of the critical and non-critical machines respectively.

3.3 Control Lyapunov Function (CLF)

Another technique to design the POD of FACTS devices is to use Control Lyapunov Function (CLF) which accomodates the nonlinear behavior of the power system. Considering the system in (12), the implicit function theorem can be utilized to get the following equivalent model [7]:

$$\dot{x} = f(x, h(x)) = \tilde{f}(x), x \in \Omega \subseteq R^{n_x} \quad (26)$$

According to theorem 2.1 in [15], x_0 the equilibrium point of the system in (26) is stable if a continuously differentiable scalar function $V(x)$ is found and does satisfy the following condition:

$$\begin{aligned} (i) \quad & V(x_0) = 0 \\ (ii) \quad & V(x) > 0, \forall x \in D, x \neq x_0 \\ (iii) \quad & \dot{V}(x) = \text{grad}(V) \cdot f(x, u(x)) < 0, \forall x \in D, x \neq x_0 \end{aligned} \quad (27)$$

As a result, if a function $V(x)$ satisfies the preceding conditions it is called a Control Lyapunov Function and can be approximated by the following expression:

$$\dot{x} = f(x, u) = f_0(x) + \sum_{i=1}^m u_i f_i(x) \quad (28)$$

The input signal ($u(x)$) for the feedback control is shown in (29):

$$u_i(x) = -\text{grad}(V) \cdot f_i(x) \quad i \in [1, m] \quad (29)$$

Selecting the energy function for a SIME system (30) it is obvious that (i) and (ii) are always satisfied.

$$V(x) = \frac{1}{2} M \omega^2 - P_m \delta - P_{emax} \cos(\delta) \cdot C_0 \quad (30)$$

where the first term in (30) is the kinetic energy and the remaining terms resemble the potential energy function. Based on (28), the CLF-based control signals for SVC, TCSC and VSC-HVDC are given below:

$$\begin{aligned} \text{Signal}_{POD} &= k_{SVC} \sin(\delta_{SIME}) \omega_{SIME} \quad (\text{for SVC}) \\ \text{Signal}_{POD} &= k_{TCSC} \sin(\delta_{SIME}) \omega_{SIME} \quad (\text{for TCSC}) \\ u_p &= k_{up} \sin(\delta_{SIME}) \omega_{SIME} \quad (\text{for VSC - HVDC}) \\ u_q &= -k_{uq} \sin(\delta_{SIME}) \omega_{SIME} \quad (\text{for VSC - HVDC}) \end{aligned} \quad (31)$$

These signals in (31) which are described in detail in [6] and [7] and will be used as input signals of the PODs in this paper. The results of each signal are shown in the next section.

4. SIMULATION RESULT

4.1. Description of Test System

The single-line diagram of the tested power system is depicted in Fig.10. It is used to show the impact of the installation of controllable devices on power oscillation damping. The system consists of eleven busses, three generators, three loads and two shunt capacitors. The three devices that will be tested are connected as follows:

- 1- SVC at bus7.
- 2- TCSC between bus7A and bus8.
- 3- HVDC at bus7 and in series with the line between bus6 and bus7.

The system without controllable devices will also be tested. The behavior and response of the system will be tested by subjecting the system to small and large disturbances, respectively.

- Small disturbance: Disconnecting (load2) at bus 8 for 100ms.
- Large disturbance: Injecting a solid 3-phase to ground fault between bus6 and bus7 and clearing the fault by removing the line after 50ms.

The simulations are performed using SIMPOW software and the figures are displayed using MATLAB. The simulation will be carried out by installing each FACTS and HVDC device separately.

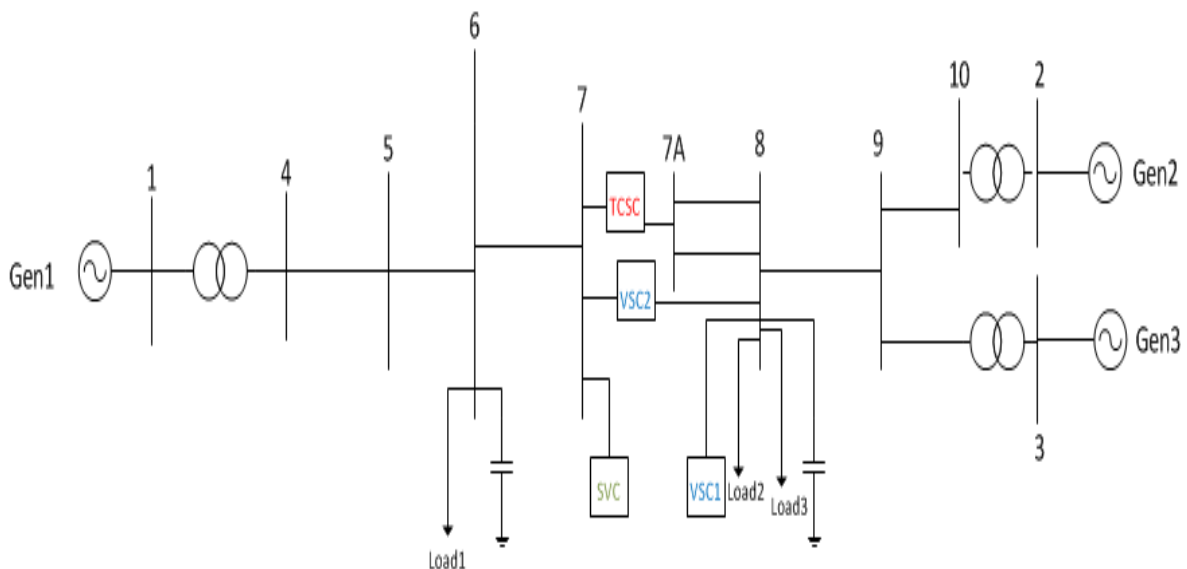


Figure 10 Studied power system with the controllable devices attached.

4.2 Modal Analysis

When running the power-flow of the system in Fig.10 without any controllable device, it is found that bus7 has a relatively low voltage (0.941pu) due to its distance from the generators. After running the linear modal analysis in SIMPOW and specifying the inter-area modes (Table.1). Clearly, the mode of interest is (15/16) since it has a frequency that is of interest (0.1Hz - 2Hz). When choosing that mode, the corresponding compass plot is

acquired (Fig.12). As shown in Fig.11, Gen1 is oscillating against Gen2 and Gen3, therefore, Gen1 is considered as a critical generator and the rest are considered as non-critical.

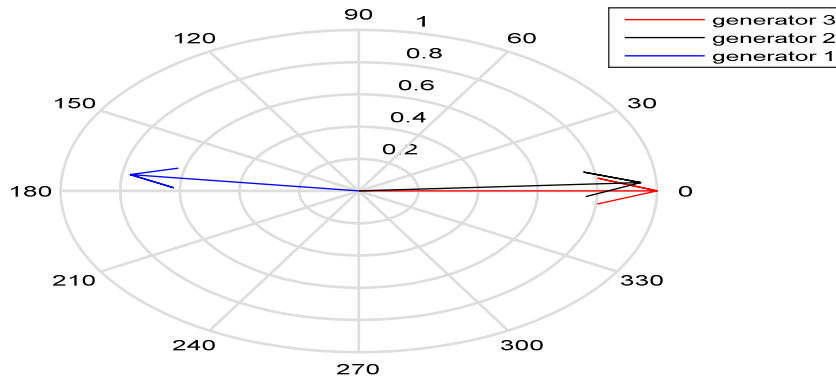


Figure 11 Compass plot of the chosen inter-area mode.

4.3 Gain Selection

A precise selection of gain is essential in the manner that it stabilizes the unstable mode while the other modes are unaffected by that gain. POD parameters and mode characteristics of SVC, TCSC and VSC-HVDC are shown in tables 1 and 2 below:

TABLE I

Comparison of Poorly Damped Mode Characteristics

Device	POD Input	Eigen Value	f (Hz)	ξ_{min}
No device	-	-0.0121+4.5718i	0.7276	0.0026
SVC	No POD	-0.0363+4.8604i	0.7736	-0.0075
	P_{78}	-0.4011+4.4169i	0.7030	0.0904
	ω_{SIME}	-1.2387 + 9.3388i	1.4863	0.1315
	CLF	-0.4883 + 4.7861i	0.7617	0.1015
TCSC	No POD	-0.0202+4.7638i	0.7582	0.0042
	P_{78}	-1.1454+9.2093i	1.4657	0.1234
	ω_{SIME}	-1.1471+9.2054i	1.4651	0.1237
	CLF	-1.1471 + 9.2054i	1.4651	0.1237
VSC-HVDC	No POD	-0.0346 + 4.4319i	0.7054	0.0078
	CLF	-0.2950 + 4.4117i	0.7021	0.0667

TABLE II

Comparison of Tuning Parameters

Device	Filter Parameters						
	Signal	# of filters	T_1	T_2	T_3	T_4	K_{POD}
SVC	P_{78}	1	0.0662	0.6394	1	1	2.86
	ω_{SIME}	1	0.375	0.1129	1	1	-100
	CLF	-	-	-	-	-	100
TCSC	P_{7AB}	2	0.0897	0.4912	0.0897	0.4912	0.39
	ω_{SIME}	1	0.2168	0.2032	1	1	-9.9
	CLF	-	-	-	-	-	20
HVDC	P_{67}	2	0.0978	0.5205	0.0978	0.5205	33.78
	ω_{SIME}	1	0.2419	0.2105	1	1	-100
	CLF	-	-	-	-	-	100

4.4 Controllability, observability and critical clearing time

The controllability and observability for each controllable device and signal used are listed in Table 3. The values were acquired using the method in [1]. The controllability depends on the input matrix (B) and the i -th mode of the left eigenvector (v_i^l), whereas the calculation of observability relies on the output signals matrix ($P_{78, \omega_{SIME}}$) of the dynamic equivalent which will yield different output matrices (C). From table 3, it is clear that the observability of the inter-area mode when the output signal is the active power between line 7 and 8 is higher for both SVC and TCSC. The reason is that in a two-area type of systems these modes have a direct relationship with the oscillation of the active power flow through the line. The calculation of critical clearing time for large disturbance of the system with and without controllable devices, and with and without POD is shown in table 4

TABLE III:

Controllability and Observability

Device	Output Signal	Controllability	Observability
SVC	P_{78}	0.2914	0.0553
	ω_{SIME}	0.2914	0.0012
TCSC	P_{7A8}	0.1180	0.0208
	ω_{SIME}	0.1180	0.0011
VSC-HVDC	P_{67}	0.4643	0.0109
	ω_{SIME}	0.4631	0.0020

TABLE IV:

Critical Clearing Times Calculation

Device	POD Input	Critical Clearing Time (s)
No device	-	0.07
SVC	No POD	0
	P_{78}	0.12
	ω_{SIME}	0.12
	CLF	0.12
TCSC	No POD	0.07
	P_{7A8}	0.20
	ω_{SIME}	0.18
	CLF	0.19
VSC-HVDC	No POD	0.05
	P_{67}	0
	ω_{SIME}	0.08
	CLF	0.08

4.5 Comparison of Different Control Strategies

In this section, the figures for each component containing the plot of the rotor angle (δ_{SIME}) of the system with different control strategies are shown. For each component, four curves will be shown, where each curve resembles a control strategy. The disturbance cases stated previously will be applied and also an extra case will be applied that is right after at the critical clearing time of the large disturbance case ($t > t_{critical}$). Where critical clearing time is the maximum time for a faulted system to be stable before going to instability [15]. Figures 12-14, shows the deviations of rotor angle when TCSC component is installed.

Figures 15-17, shows the deviations of rotor angle when SVC component is installed. Figures 18-20, shows the deviations of rotor angle when VSC-HVDC component is connected. Figure 21, compares between all devices and no-device case and when the control strategy used is CLF since it theoretically gives the highest damping ratio. Figure 22, is similar to 21 but now it compares between the devices when a large disturbance is injected to the system.

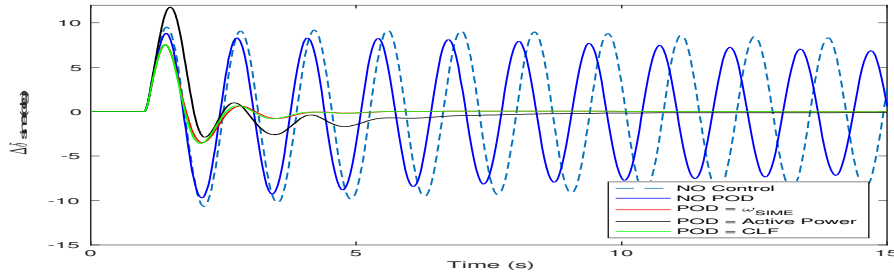


Figure 12 Deviations of rotor angle in case of TCSC small disturbance.

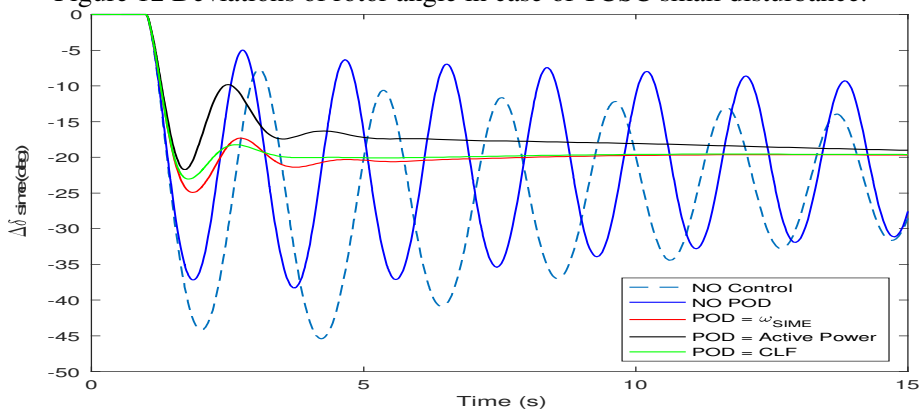


Figure 13 Deviations of rotor angle in case of TCSC large disturbance.

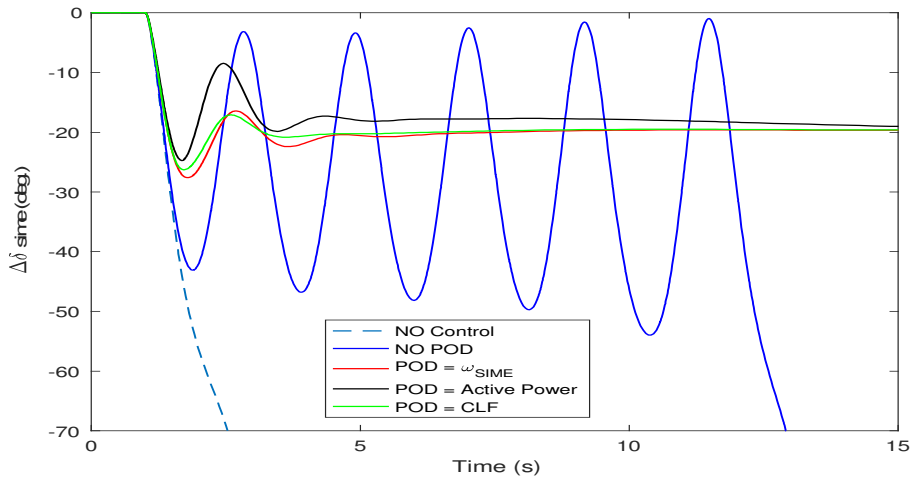


Figure 14 Deviations of rotor angle in case of TCSC large disturbance at $t = t_{critical} + 0.01$.

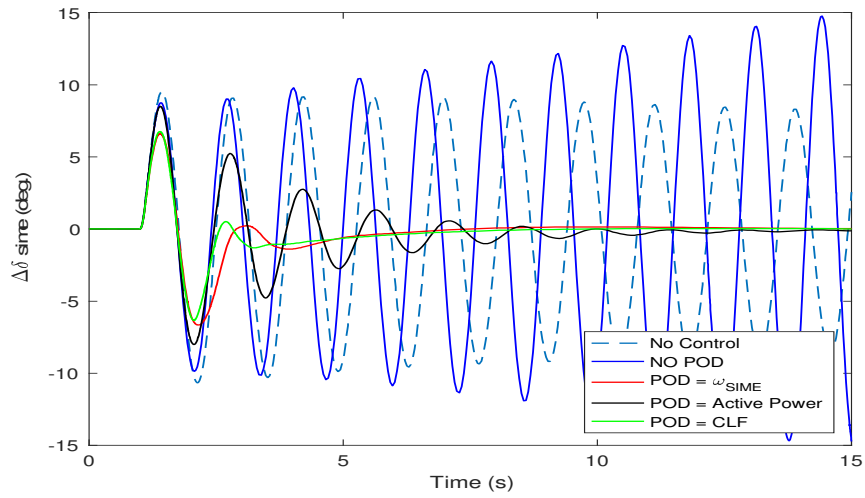


Figure 15 Deviations of rotor angle in case of SVC small disturbance.

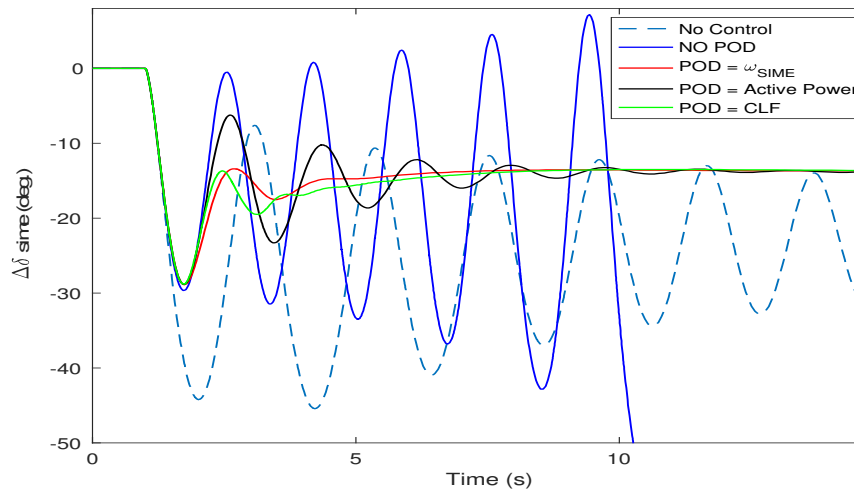


Figure 16 Deviations of rotor angle in case of SVC large disturbance.

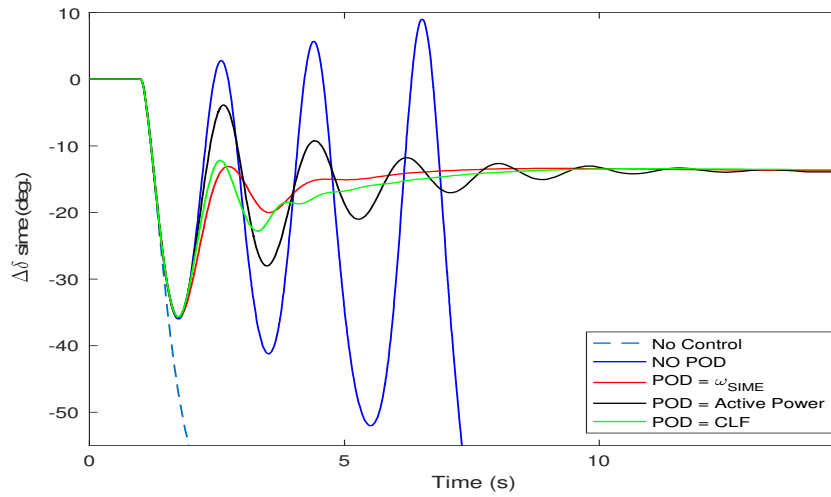


Figure 17 Deviations of rotor angle in case of SVC large disturbance at $t = t_{critical} + 0.01$.

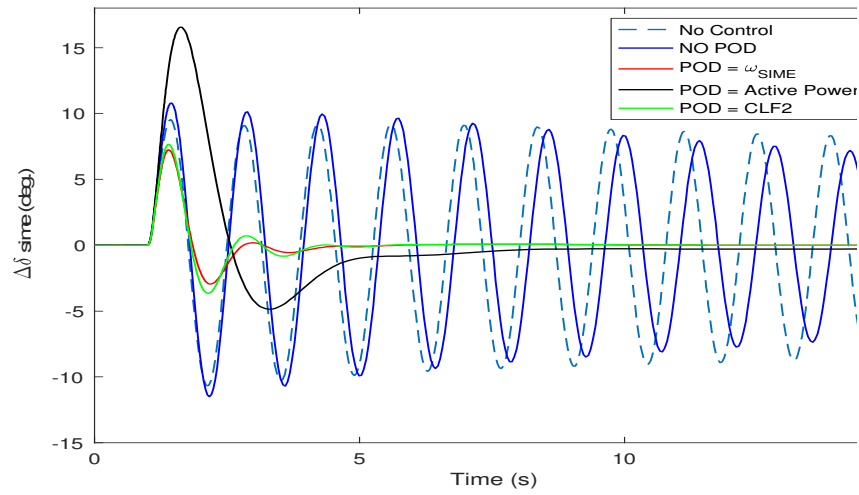


Figure 18 Deviations of rotor angle in case of HVDC small disturbance.

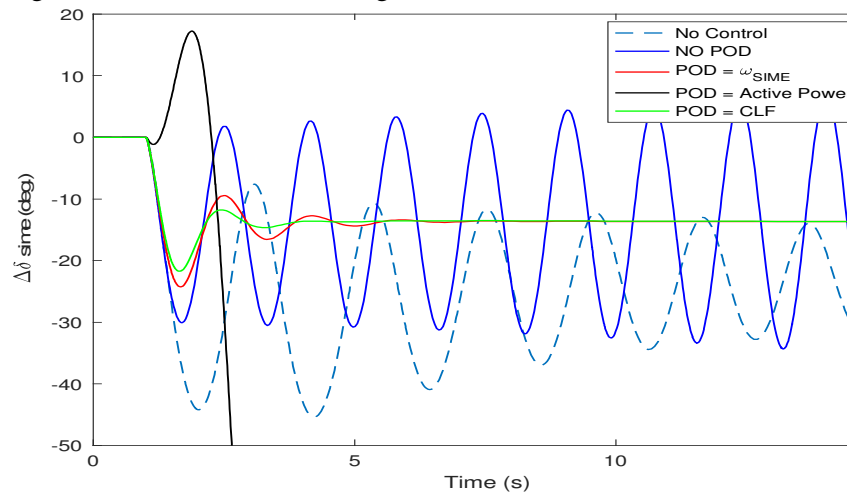


Figure 19 Deviations of rotor angle in case of HVDC large disturbance.

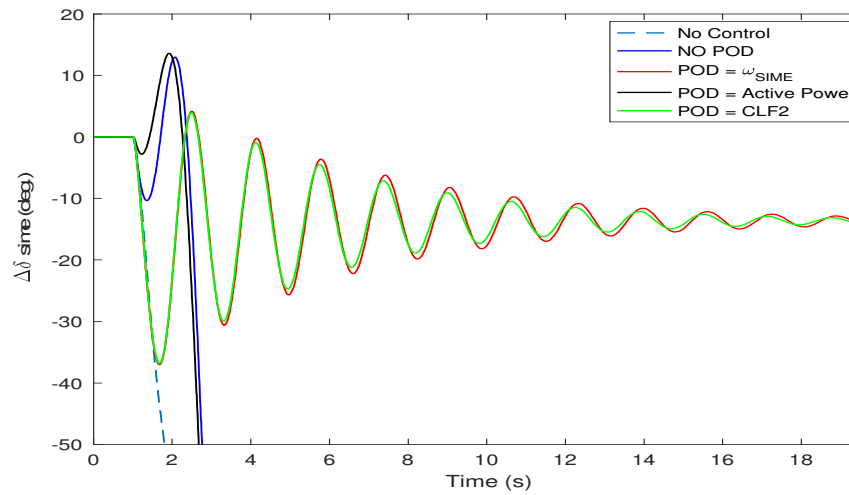


Figure 20 Deviations of rotor angle in case of HVDC large disturbance at $t = t_{critical} + 0.01$.

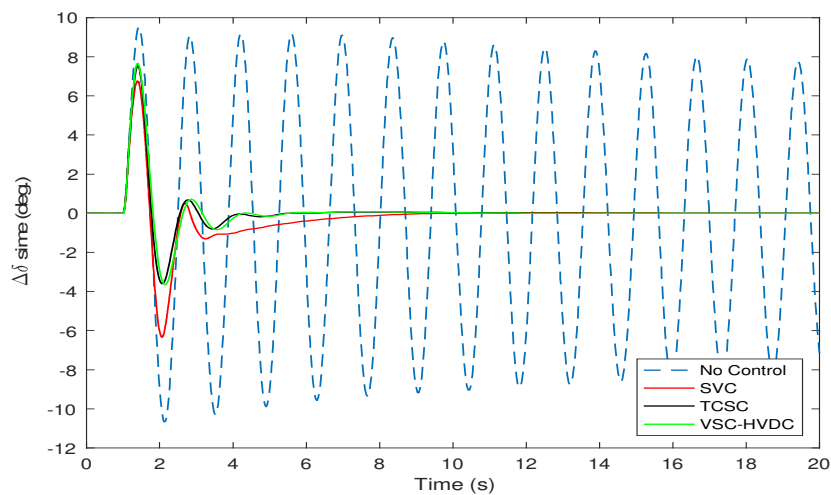


Figure 21 Comparison of SIME of all assigned devices obtained from PO of CLF based law in case of small disturbance.

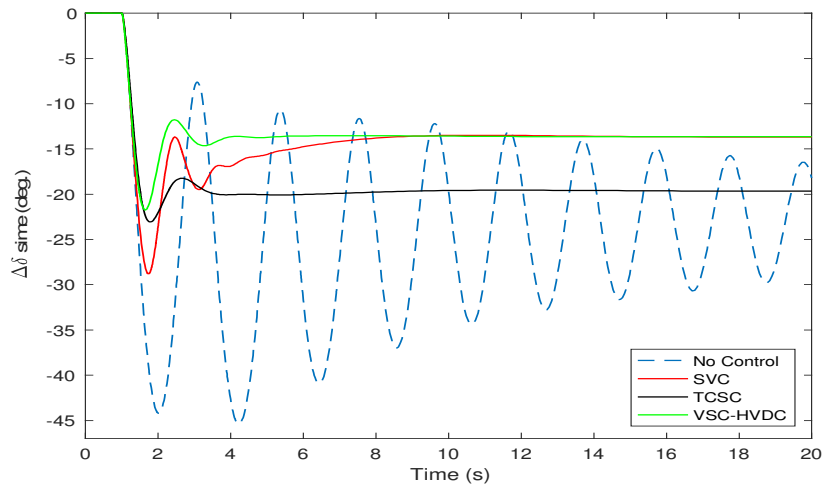


Figure 22 Comparison of SIME of all assigned devices obtained from POD of CLF based law in case of large disturbance.

4.6 Applying N-2 Criterion

The logical number of contingencies depends on many factors. Among them are the number of components, the depth of the analysis and the severity of the disturbance [12]. To keep the system in secure operation, transmission grids have to meet the N-1 criterion which, if achieved, assures the system continuity of operation even if a component was suddenly lost. However, the N-2 contingency standard secures the system even if two components were lost. The curves in Fig.23, Fig.24 and Fig.25 were drawn after applying the following two disturbances:

- (i) Injecting a solid 3-phase to ground fault between bus6 and bus7 and clearing the fault by removing the line after 50ms.
- (ii) Disconnecting (load2) at bus 8 after 4ms of the occurrence of the first fault.

Thus, (i) is the N-1 disturbance and (ii) is the N-2 disturbance. The two disturbances does not occur at the same time as such occasions are very rare to happen. Sometimes it is referred to our case here as N-1-1 disturbance, indicating the sequential occurrence of faults.

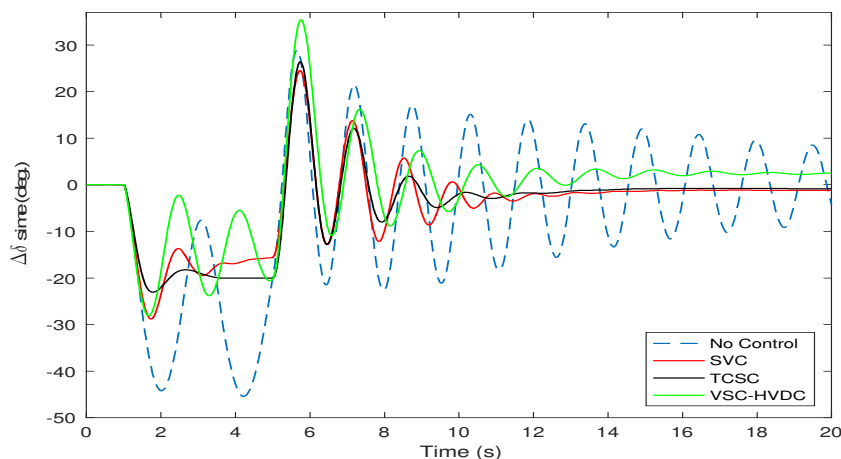


Figure 23 N-2 disturbance when POD=CLF.

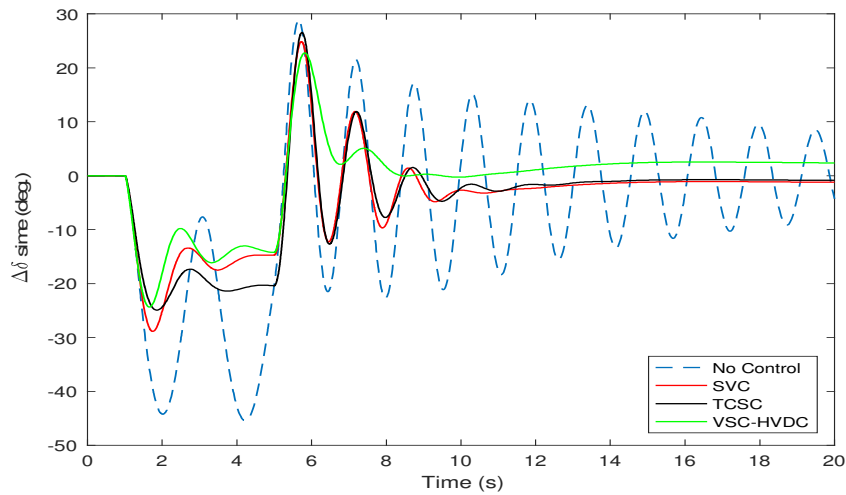


Figure 24 N-2 disturbance when $POD = \omega_{SIMÉ}$.

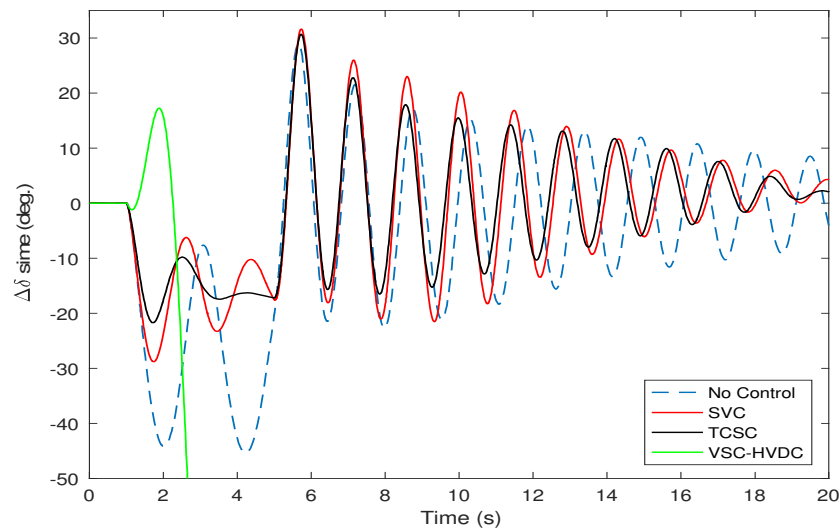


Figure 25 n-2 disturbance when $POD = \text{active power}$.

5. DISCUSSION

When looking at Fig.12 and Fig.13, one can notice the differences in severity between small and large disturbances on the rotor angle fluctuations. Fig.12 through 20, show the slight increase in transient and small signal stability when FACTS and HVDC devices were added. However, the significant improvement was noticeable when these devices were controlled by the power oscillation damper signal. Fig.14, Fig.17 and Fig.20 show how the system went unstable in the case of no POD, whereas stability was maintained when POD signals were introduced. In other words, the critical clearing time was elongated thus the reliability of the system has been enhanced. From the simulation results also, it is deduced in the case of TCSC and HVDC, that CLF was the best POD signal for all disturbance cases due to the high gains provided. Whereas in the case of SVC, both $\omega_{SIMÉ}$ and CLF have a similar performance and showed a better and faster damping than the active power signal. Fig.21 and Fig.22 compare the performance of all devices when CLF method was applied and from the curves it can be seen that TCSC outperforms the rest of devices. In Fig.23, Fig.24 and Fig.25 another disturbance was injected and TCSC again managed to have the fastest damping among other devices. Regarding control signals, generally speaking, $\omega_{SIMÉ}$ showed the best pattern in damping rotor angle deviations. However, this comes on the price of the high gain needed for the lead-lag filters of the global signal as well as the expenses of installing communication equipment. The lower gain value required for the

active power (P_{AC}) signal is attributed to the high observability of this local signal. Also, the location of the active power signal is crucial and it was chosen to be the power through the line between bus 7 and 8 since this line connects the two regions in the system. Furthermore, from the power flow, bus 7 has the lowest voltage and bus 8 has the lowest angle. For the HVDC case, the active power through the line connecting bus 6 and bus 7 was chosen to overcome the large-disturbance occurring at that line since the voltage level is sensitive more to changes on the active power flow. In theory, it is better to control the active power by the line connecting two system areas which will eventually provide a more resilient damping of inter-area oscillations. The main purpose of choosing a specific regulators and controllers for the POD signal, is their sensitivity to eigenvalues of the linearized power system [13].

6. CONCLUSION

In this paper, the impact of two FACTS devices and one HVDC system on small-signal and transient stability of a power systems was analyzed. Three Power Oscillation Damping (POD) supplementary signals was designed and used to control the devices and improve the system when subjected to inter-area oscillations. Two linear PODs were designed based on residue method and one nonlinear POD was designed using Control Lyapunov Function (CLF). The performance of the devices was assessed when injecting different POD signals. The simulation results showed how FACTS and HVDC outperform when control strategies are applied. The results also showed an impressive contribution of controlled FACTS and HVDC devices in protracting system failures by increasing the system survival time after contingencies. The ability of the controlled devices to recuperate the system when faults occur was also demonstrated. In terms of analytical studies and due to nonlinearity, CLF was expected to provide the best damping, however, this is not the case in our simulation. The reason is that when applying the linear PODs (P_{AC} & ω_{SIME}), the eigenvalues location relies on the tuning of the feedback gain which was calculated using a linearized system model which, most probably, do not correspond to the optimal gain for the non-linear system model. In other words, tuning the filter based on a linearized model was the reason behind the lagging performance of CLF in our results. However, CLF signal performance was still better than (P_{AC}) A future work for this paper can be extended to solve the issue of calculating the POD gains using the residue method which is a rough linearised model of the non-linear behavior of our system model.

ACKNOWLEDGMENT

The author would like to acknowledge the support and supervision of Dr. Mehrdad Ghandhari, Full Professor, and Mr. Muhammad Taha Ali, PhD student, at Electrical Engineering Department, KTH Royal Institute of Technology. Additional appreciation goes to KTH Royal Institute of Technology for supporting this research and providing the tools needed to accomplish the project.

REFERENCES

- [1] A. Hamdan and A. Elabdalla, "Geometric measures of modal controllability and observability of power system models", *Electric Power Systems Research*, vol. 15, no. 2, pp. 147-155, 1988.
- [2] Asawa, S. and Al-Attiyah, S. (2016). Impact of FACTS device in electrical power system. 2016 International Conference on Electrical, Electronics, and Optimization Techniques (ICEEOT).
- [3] E. Larsen, N. Miller, S. Nilsson and S. Lindgren, "Benefits of GTO-based compensation system for electric utility application", *IEEE Transactions on Power Delivery*, vol. 7, no. 4, pp.2056-2064, 1992.
- [4] M Ghandhari, G. Andersson, M. Pavella, D.Ernst: "A control strategy for controllable series capacitor in electric power systems". *Automatica* 37, pp. 1575–1583,2001
- [5] Latorre, H.F., and M. Ghandhari. "Improvement of Power System Stability by Using A VSC-Hvdc". *International Journal of Electrical Power & Energy Systems* 33.2 (2011): 332-339.
- [6] Mehrdad Ghadhari, Hector Latorre, Lennart Angquist, Hans Peter Nee, Dirk Van Hertem, "The Impact of FACTS and HVDC Systems on Transient Stability and Power Oscillation Damping", *Electric Power Systems*, Royal Institute of Technology.
- [7] M. Ghandhari, G. Andersson, I.A. Hiskens, "Control Lyapunov functions for controllable series devices", *IEEE transactions on power systems*, vol. 16, no. 4, Nov.2001.
- [8] M. Ghandhari and G. Andersson, "Two various control laws for controllable series capacitor (CSC)".
- [9] STRI, SIMPOW- A Digital Power System Simulator, ABB Review No. 7, 1990.
- [10] Therond et al: "Modeling of power electronics equipment (FACTS) in load flow and stability programs", 1st ed. [Paris] [CIGRE], 1999.
- [11] Yang, N., Liu, Q., LicCalle, J., TCSC Controller Design for Damping Interarea Oscillations, *Power Systems*, *Transactions on Power Systems*, Vol. 13, No. 4, August 1991.
- [12] A. Tiwari and V. Ajjarapu, "Contingency assessment for voltage dip and short term voltage stability analysis", 2007 iREP Symposium - Bulk Power System Dynamics and Control - VII. Revitalizing Operational Reliability, 2007.
- [13] Y. Song and A. Johns, *Flexible ac transmission systems (FACTS)*, 1st ed. London: Institution of Electrical Engineers, 2008.
- [14] A. Alahmed, *Cost Comparison Between Bi-polar HVDC Lines and 3-phase HVAC Lines*, 1st ed. Dhahran, Saudi Arabia: King Fahd University of Petroleum and Minerals, 2018.
- [15] Y. Shirai, M. Mukai, T. Sakamoto and J. Baba, "Enhancement Test of Critical Clearing Time of One-Machine Infinite Bus Transmission System by Use of SFCL", *IEEE Transactions on Applied Superconductivity*, vol. 28, no. 4, pp. 1-5, 2018.